Sonochemistry

DOI: 10.1002/anie.201002069

Selective Ultrasonic Cavitation on Patterned Hydrophobic Surfaces**

*Valentina Belova, Dmitry A. Gorin, Dmitry G. Shchukin, and Helmuth Möhwald**

Ultrasound can create cavitation bubbles that upon collapse cause extreme temperatures and pressures. Sonochemistry therefore carries much promise as an environmentally friendly method to carry out chemical processes at ultrahigh temperatures (ca. 5000 K), and pressures (ca. 1000 atm),[1–6] but with a reactor at near-ambient conditions.[7,8] The extraordinarily high cooling rates also enable preparation of materials far from equilibrium; for example, nanoparticles for catalysis, optics, and electronics.[9–11] Herein we demonstrate semiquantitatively that nucleation of gas bubbles at surfaces can be controlled by the surface energy. Patterning of surfaces by molecular assembly thus enables formation of lateral patterns with well-defined nanoscopic roughness and chemistry, opening possibilities for new surface chemistry and physical studies of defined bubble nucleation. A model is presented that takes into account the competition between surface energy and the acoustic energy to inhibit and induce cavitation, respectively.

In recent years, sonochemistry has developed from an exotic art into a most promising discipline in materials science. The process has also been used to create defined surfaces with specific roughness and surface chemistry for strong adhesion or for defined electrochemistry and catalysis.[12,13] It is also used routinely in industry and also in most laboratories for the cleaning of surfaces.[14] However, the question is only rarely asked as to whether the surface also influences the cavitation process. It should be possible to control surface treatment by the control of surface energies.[15,16] This should not only hold for planar surfaces, but also for surfaces of microparticles and their dispersion and for the treatment of mixed solids where one component should be dispersed, for example, in separation chemistry or in preparing microporous solids.[17]

A most promising way to access the influence of surface energies is to make use of microprinting techniques. In this way, micrometer-sized hydrophobic areas can be prepared next to hydrophilic regions and maintain bulk conditions, thus allowing the two types of surfaces to be compared under identical conditions.[18–21] This also holds for the acoustic pressure, as ultrasonic wavelengths used for sonochemistry are typically longer than 1 mm.[1–5,22] These conditions and techniques are applied herein: we will concentrate on understanding the mechanism, but keep in mind that this is also a way to prepare microroughnesses and surface chemistry on well-defined and preselected areas, which is useful for a broad range of applications.

Scenarios that compare bubble formation on hydrophobic and hydrophilic surfaces and in the bulk are given in Figure 1.[6,23,24] To explain the surface influence on bubble nucleation, we use a continuum approach in analogy to that used by Brennen.[25] The energy of a bubble with curvature radius R on a surface contains a positive surface-energy term with liquid surface tension σ and a geometrical function $g(\theta) = 2 + 3\cos\theta - \cos^2\theta$ that depends on the contact angle θ[26] and a volume term $E_b = -\pi/3\, R^3 g(\theta) P$. The pressure $P = P_A + P_G + P_V$ is composed of the acoustic pressure P_A (which dominates in this work),[27] the partial pressure P_G of a gas,

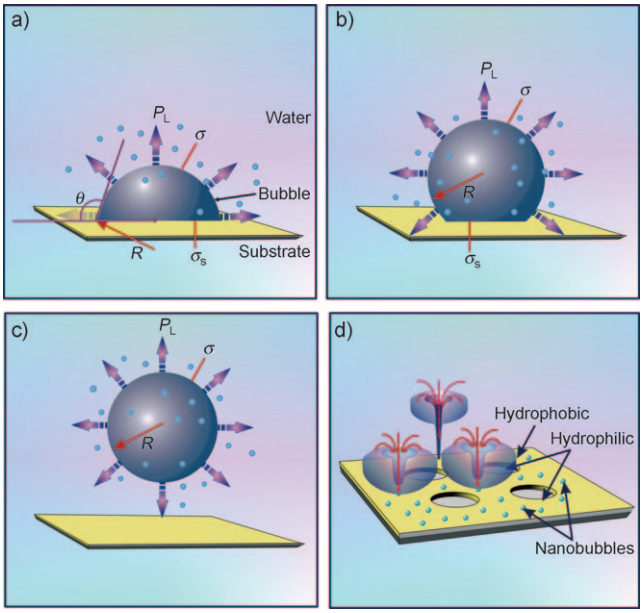

Figure 1. Comparison of nucleation and growth of a cavitation bubble at a) a hydrophobic and b) a hydrophilic surface, and c) in bulk. The pressure P performing the volume work is given by the vapor pressure P_V of the liquid, the gas pressure P_G, and the acoustic pressure P_A being in excess of the external pressure P_L (see text). d) Mechanism of the selective gas-bubble nucleation on the hydrophobic/hydrophilic microstructured surface.

[*] Dr. V. Belova, Dr. D. A. Gorin, Dr. D. G. Shchukin, Prof. H. Möhwald
Department of Interfaces
Max Planck Institute of Colloids and Interfaces
Am Mühlenberg 1, 14476 Potsdam-Golm (Germany)
Fax: (+49) 331-567-9202
E-mail: helmuth.moehwald@mpikg.mpg.de
Homepage: http://www.mpikg.mpg.de/english/04-interfaces/director/contact/index.html

[**] The work was supported by the BMBF, the EU sixth framework. The authors thank Dr. J. Hartmann, Dr. T. Borodina, R. Pitschke, and A. Heilig for help with SEM and AFM measurements and Dr. B. Porohonski for help with *ImageJ* Software. We thank A. Kretzchmar and J. von Szada-Borryszkowski for the pre-treatment of the samples for all experiments.

Supporting information for this article is available on the WWW under http://dx.doi.org/10.1002/anie.201002069.

and the vapor pressure of the liquid (P_V).[28] Compared to this volume work with $P_A \geq 1$ atm, other contributions may be negligible. The nucleation energy barrier is given by Equation (1):

$$\Delta E = \frac{4\pi}{3}\frac{\sigma^3}{P^2}\, g(\theta) \qquad (1)$$

An example that uses typical values of P, σ, and $g(\theta)$ is given in Figure 2. It is remarkable that for equilibrium shape, the geometrical factor $g(\theta)$ for both energy contributions is

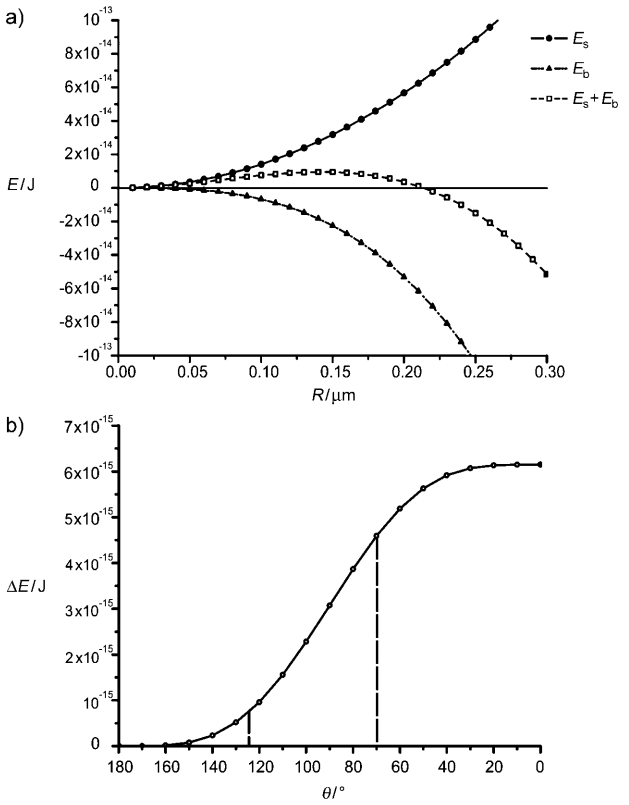

Figure 2. a) Dependence of the volume work (E_b), the surface energy (E_s), and superposition result ($E_s + E_b$) on the radius of a gas bubble. b) The nucleation energy barrier as a function of contact angle θ derived from the maximum in $E_s + E_b$. The center regions marked by the vertical lines correspond to the contact angles applied in this work. For the calculation, the surface tension of water (72 mN m^{-1}) and the pressure 10 atm, roughly corresponding to the highest ultrasonic powers, were used.

the same, and for the range of contact angles used in our experiments varies by a factor of 5. In our practical situation, the energy barrier is about a factor of 1.5 smaller than expected in the bulk ($\theta = 0°$) and very high ($> 10^6\, kT$). Therefore, it is expected that preferential nucleation occurs on surfaces, and especially on hydrophobic surfaces, but thermal nucleation is improbable. We do not dwell on the question as to whether bubbles result from adventitious events that then concentrate on the hydrophobic surface for further growth, which in other fields is called secondary nucleation, or if they result from a rare primary event (see below).

Aluminum was selected as a soft metal that enables the (indirect) measurements of cavitation rate owing to the impact of a jet formed upon bubble collapse. The aluminum surface was stamped with a mixture of *n*-octadecylphosphonic acid and octadecanethiol. After an etching process, excess adsorbed amphiphilic material on a hydrophobic surface with cylindrical hydrophilic areas was obtained (Supporting Information). Figure 3a,b shows electron micrographs of an

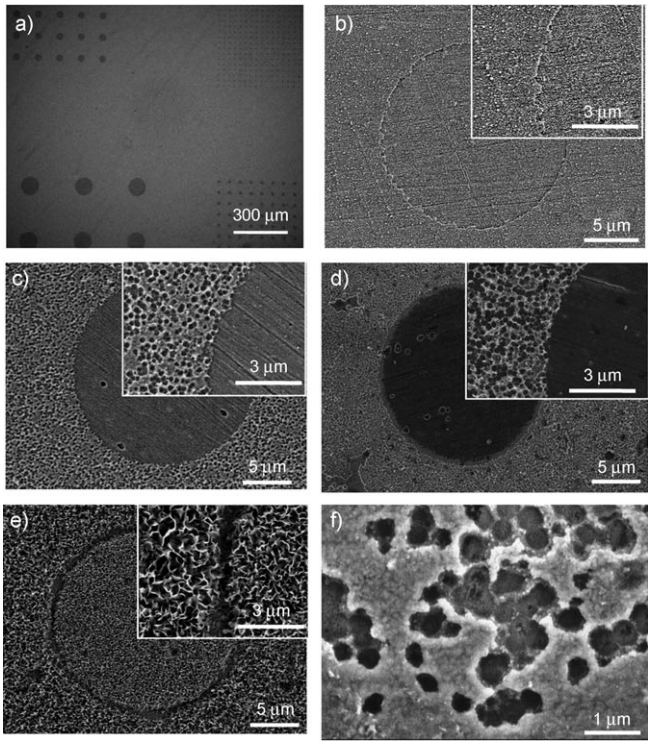

Figure 3. ESEM (a) and SEM (b–f) images of the patterned aluminum plate before ultrasonic treatment (a, b) and after ultrasonic treatment: c) at 10 min of sonication, d) at 30 min of sonication, e) high magnification of the hydrophobic surface with pits at 30 min of sonication, and f) at 40 min of sonication. The inner circular area is hydrophilic, and the outer part is hydrophobic. Treatment temperature: 340 K. See text for further details.

aluminum surface at different magnifications. The dark areas are hydrophilic with a contact angle (measured separately) of 70°. They exhibit only a small area fraction, thus the macroscopically measured angle corresponds essentially to that of the hydrophobic area, with a contact angle of 125°. For ultrasonic treatment, a flat sonotrode (3.14 cm^2 area) was placed 1.5 cm above the aluminum plate in a water bath fitted with a thermostat (±1 K). The wave (20 kHz) impinged normally at the surface, and the ultrasonic power density was laterally homogeneous and could be varied between 29 and 51.3 W cm^{-2}. The images of the ultrasonically treated surfaces (Figure 3c,d), reveal that, whereas the hydrophilic areas remain unchanged, the hydrophobic areas are obviously impacted by ultrasonic treatment. The pits developed have dimensions of less than 0.5 μm (Figure 3e). Images such as those in Figure 3c,d are obtained over the

whole area of the printed surface, thus enabling formation of well-defined flat areas in an environment of uniform nanoroughness (Supporting Information, Figure S3).

Upon extending the treatment further, the hydrophilic areas are also impacted, but the boundary between the hydrophilic circular area and hydrophobic surrounding remains visible (Figure 3 f). The drastic change in surface texture in this case may be due to the fact that initially formed pits present secondary nucleation sites.[24,29] Altogether, these results confirm the expectation according to Equation (1) that a higher contact angle causes a lower energy barrier, and thus cavitation occurs predominantly at the hydrophobic surface.

To quantify the observed pit formation, electron micrographs obtained at various temperatures, sonication times, and ultrasonic power were analyzed; the number of pits counted per reference area ($7 \times 5\ \mu m^2$) is given in Figure 4. It can be seen that there is a lag phase, then a steep increase in the number of pits per time. This lag phase may indicate that initially created nanobubbles assemble on the hydrophobic surface to form the nucleus, as described by Equation (1). Beyond a maximum there is the merger of pits, which makes quantification meaningless. However, clearly observes an increase of the nucleation rate with temperature by a factor of two can be clearly observed (compare the difference between 5 and 10 min) for the temperatures 293 K and 340 K and with ultrasonic power (Supporting information, Figure S2). For the ultrasonic power, the changes are more pronounced at 293 K, indicating the proximity of a threshold regarding the rate as a function of power. The power arises in the acoustic pressure P_A, which however varies only by 30% owing to the square-root dependence on power.

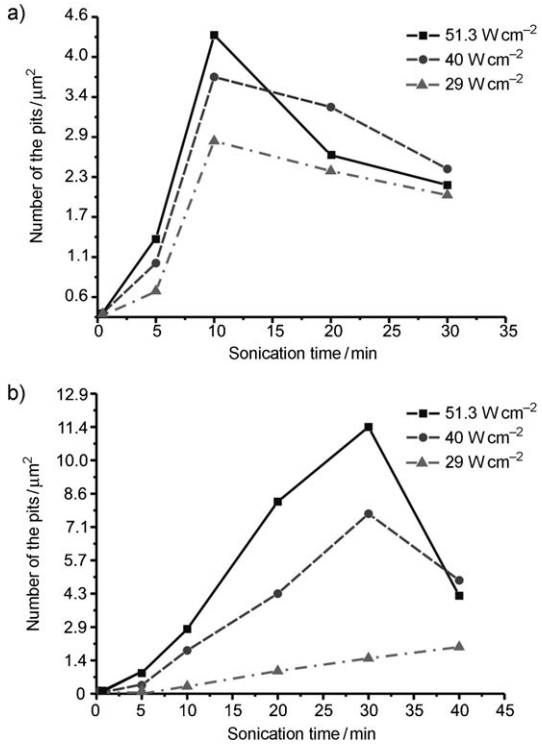

Figure 4. Plot of the pit density for different ultrasonic irradiation power as a function of sonication time: a) 340 K; b) 293 K (diameter of hydrophilic holes is 19.2 µm, interspacing is 67.2 µm). The density is derived for the hydrophobic areas, and it is negligible on the hydrophilic areas for sonication times below 30 min.

To confirm that ultrasound is the only cause of the changes to the surface, further experiments were carried out:

- It is known that also heating a surface may create corrugations. However, even after extended boiling, we could not detect the well-defined pits found with ultrasound (Supporting Information, Figure S4b).
- Using plasma treatment, the surfactant could be removed again, and this was verified by IRRA spectroscopy and contact-angle measurements (angle of less than 20°). In this case, the impact of ultrasound on the two previously different surfaces became indistinguishable (Supporting information, Figure S4a).

We also tested the stability of the pattern during ultrasonic irradiation. Within the treatment time of 10 min, the contact angle at highest power typically changed from 125° to 120°, but for a duration of 60 min, it could be reduced to 70 degrees. Therefore for a quantitative study, only the first minutes of treatment are useful, and for long-term treatment more stable coatings or structured films should be developed.

Even though we did not determine any threshold for cavitation as might be expected by nucleation theory, we should comment on the importance of different parameters varied here in conjunction with Equation (1). The strong dependence on contact angle has been discussed before. Another important factor is the surface tension σ, which arises with a cubic power. σ may be varied, for example, by impurities or particles removed from the surface, and this may explain why at later times hydrophilic areas are also impacted. Therefore our finding that bubble nucleation predominates with higher θ, and is accelerated by increased temperature (mainly by a decrease in σ) and by ultrasonic power is in agreement with the model.

As mentioned above, the model of thermally induced nucleation is not very probable in view of the high energy barriers involved. Instead we propose a slightly different model: The barrier in Figure 2 is a minimum value with regard to the time dependence, as it corresponds to the maximum pressure of acoustic rarefaction. During the pressure cycles, ΔE decreases and disappears upon compression, leading to a very small nanobubble that is stabilized by the Laplace pressure, and is again increased by the acoustic energy input. The latter increases more and faster if the opposing surface tension term in Figure 2 is decreased, for example by local heating, and this accelerates nucleation. This model will have to be verified in future studies by varying the surface tension and ultrasonic frequency to arrive at a quantitative and predictive way of surface modification.

In comparing nucleation on a surface and in bulk, the following experimental facts must be taken into account:

- The acoustic pressure at the surface and in the bulk might drastically deviate owing to reflection of the wave at a surface. This may not be relevant considering the range of micrometers near the surface, but for distances of a fraction of the wavelength (centimeters), the pressure is different, and bubbles created there may still impact the surface.

- Although the temperature of the system was controlled with a thermostat, there may be temperature gradients between surface and bulk and between the center and wall of the reactor. This may explain the slower nucleation rate at the beginning of sonication.
- There may be corrugations and inhomogeneities on the surface that further reduce the energy barrier.

It is also remarkable that the pits on a surface are very small and confined on the hydrophobic areas, although it would be expected that the bubbles have diameters around 100 μm before collapse. This finding indicates that the impact is confined to the center of a bubble, which also corresponds to the spot of nucleation. This may indicate the influence of a jet (Figure 1 d), but shockwaves may also possess high energy and yield small pits if they develop close to the surface.[30,31] Later decreasing the contact angle by sonication also decreases the differences between both types of surfaces, thus also enabling jet and shockwave formation above the circular areas. At this point we should also stress that we aimed at and achieved preparing surfaces that are flat at the nanometer level and distinguished mostly by the ultrathin coating. The etching caused a depth difference of less than 100 nm, and the lower hydrophilic areas cannot provide a gas reservoir as is the case in the experiments carried out by Lohse et al. on cavitation in hydrophobic crevices.[32]

In conclusion, we have shown that by patterning a surface, a model of heterogeneous nucleation of cavitation bubbles can be formulated. The following impact on surfaces was qualitative as expected regarding varying surface energies, temperature, and ultrasonic power. To verify these models, more quantitative analysis and theoretical modeling of the growth kinetics will be needed.

We concentrated herein on nucleation of cavitation, but the method of chemically patterning without changing the surface energy is also most suitable to study further bubble growth: these bubbles would be expected to grow towards diameters of 100 μm, and the contact area may be limited well below this size, thus allowing the three-phase boundary to be studied. This provides an additional control of surface treatment (or way of preparation) by ultrasound. Further dedicated and quantitative studies should thus pave a way to make use of ultrasound to modify the geometry and chemistry of surfaces and films, to leach these preferentially, or to nucleate bubbles on microparticles with a defined surface. This would be a major step towards making this a technology with broad applications in chemistry and materials science.

Experimental Section

Materials: The stamp material, Sylgard-184 poly(dimethylsiloxane) (PDMS), and curing agent were obtained from Dow Corning GmbH. It was mixed in a 1:10 curing agent/pre-polymer ratio. Stamp replication was performed in contact with a silicon master ($10 \times 10\ mm^2$) purchased from GeSiM mbH. The aluminum alloy AA2024, provided by EADS Deutschland, was used as a model metal substrate. For all experiments, aluminum samples with the size of $10 \times 20\ mm^2$ were polished and cleaned with methanol in an ultrasonic bath for 15 min. A 100 nm thick aluminum layer was deposited by evaporation immediately prior to use. According to Ref. [33], the time between aluminum evaporation and SAM deposition should be kept very short. Delay times were therefore generally not longer than about two hours. Octadecanethiol (ODT, 96% purity, Alfa Aesar), *n*-octadecylphosphonic acid (ODPA, Alfa Aesar), phosphoric acid, nitric acid, acetic acid, and ethanol were used as received. The ink solution was freshly prepared before each set of experiments by dissolving ODT and ODPA in ethanol. Dissolution was supported by immersion in an ultrasound bath for about 10 min. All aqueous solutions were prepared using deionised Millipore Milli-Q water.

Microcontact printing and etching (Supporting Information, Figure S1): A mixed solution of ODPA (10 mM in ethanol) and ODT (2 mM in ethanol) was filtered and dropped onto the PDMS stamp. The stamps (about $10 \times 10\ mm^2$) were equilibrated for 1 min in the ink solution. The excess solution was removed under a steam of filtered N_2 gas. Stamping was performed manually by using tweezers for stamp handling and by taking advantage of the natural stamp–substrate adhesion. Contact times were 10 min. Printed aluminum samples were post-treated on a hot plate (70 °C) for 10 min. The samples were etched at room temperature in open polyethylene containers using a freshly prepared etching bath. The etchant (aluminum etchant type "A") is a combination of phosphoric, acetic, and nitric acids and water in a ratio 16:1:1:2.[34]

Scanning electron microscopy (SEM) was performed with a Gemini Leo 1550 instrument at an operating voltage of 3 keV to study the morphology of aluminum. Samples were sputtered with gold.

Field-emission environmental microscopy (ESEM) was performed with a high-resolution low-vacuum FEI Quanda 600 FEG instrument at an operating voltage 30 kV with extended low-vacuum capabilities.

Contact-angle (CA) measurements: The hydrophobicity of the fabricated prints on the aluminum plates was investigated by measuring water CAs with a contact angle meter (Software DSA 1, Krüss GmbH) at room temperature. 3 μL of deionised Millipore Milli-Q water droplets were placed on the fabricated surfaces and apparent CAs were observed. CAs were measured at three different positions for each test sample.

IR spectra were acquired with a Bruker IFS 66 FTIR spectrometer equipped with an external reflectance unit containing a Langmuir trough setup. The infrared beam was directed through the external port of the spectrometer and was subsequently reflected by three mirrors in a rigid mount before being focused on the sample surface. An AKRS-5 wire grid polarizer was placed into the optical path directly before the beam hit the sample surface. The reflected light was collected at the same angle as the angle of incidence. The light then followed an equivalent mirror path and was directed onto a narrow band mercury cadmium telluride detector, which was cooled by liquid nitrogen. The entire experimental setup was enclosed to reduce relative humidity fluctuations. For all measurements at $40\ mN\,m^{-1}$, p-polarized radiation was used at an angle of incidence of 70°. A total of 128 scans were acquired with a scanner velocity of 20 kHz at a resolution of $8\ cm^{-1}$.

The open-source software *ImageJ* is designed for the analysis of SEM imagery of structure and is released under the GPL license.[35] The ultrasonic processor UIP1000 hd from Hielscher Ultrasonics was used with a cooling system inside the converter. The experiments were carried out at an excitation frequency of 20 kHz and power of 29, 40, and $51.3\ W\,cm^{-2}$. During all experiments, the patterned aluminum samples were fixed perpendicular to the ultrasonic tip at a distance of 15 mm.

Received: April 7, 2010
Revised: June 25, 2010
Published online: August 19, 2010

Keywords: nanostructures · nucleation and growth · sonochemistry · surface chemistry · ultrasonic cavitation

[1] K. S. Suslick, L. A. Crum, *Sonochemistry and Sonoluminescence*, *Vol. 1*, Wiley-Interscience, New York, **1997**.
[2] Y. T. Didenko, W. B. McNamara, K. S. Suslick, *J. Am. Chem. Soc.* **1999**, *121*, 5817.
[3] J. Rae, M. Aschokkumar, O. Eulaerts, C. von Sonntag, J. Reisse, F. Grieser, *Ultrason. Sonochem.* **2005**, *12*, 325.
[4] M. Ashokkumar, R. Hall, P. Mulvaney, F. Grieser, *J. Phys. Chem. B* **1997**, *101*, 10845.
[5] T. J. Mason, J. P. Lorimer, *Sonochemistry: Theory, Applications and Uses of Ultrasound in Chemistry*, Harword, Chichester, UK, **1988**.
[6] J. W. Westwater, *Advances in Chemical Engineering*, *Vol. 1*, Academic Press, New York, **1956**, Chapter 1.
[7] C. R. Thomas, C. H. Farny, C. C. Coussios, R. A. Roy, R. G. Holt, *Acoust. Res. Lett. Online* **2005**, *6*, 182.
[8] L. Rayleigh, *Philos. Mag.* **1917**, *34*, 94.
[9] S. I. Nikitenko, Y. Koltypin, V. Markovich, E. Rozenberg, G. Gorodetsky, A. Gedanken, *Angew. Chem.* **2001**, *113*, 4579; *Angew. Chem. Int. Ed.* **2001**, *40*, 4447.
[10] V. Belova, H. Möhwald, D. G. Shchukin, *Langmuir* **2008**, *24*, 9747.
[11] D. G. Shchukin, H. Möhwald, *Phys. Chem. Chem. Phys.* **2006**, *8*, 3496.
[12] M. Ashokkumar, F. Grieser, *Rev. Chem. Eng.* **1999**, *15*, 41.
[13] N. A. Dhas, K. S. Suslick, *J. Am. Chem. Soc.* **2005**, *127*, 2368.
[14] A. E. Crawford, *Ultrasonics* **1967**, *5*, 150.
[15] M. Jaschke, H.-J. Butt, H. E. Gaub, S. Manne, *Langmuir* **1997**, *13*, 1381.
[16] N. Bremond, M. Arora, C.-D. Ohl, D. Lohse, *Phys. Rev. Lett.* **2006**, *96*, 224501.
[17] H.-M. Xiong, D. G. Shchukin, H. Möhwald, Y. Xu, Y.-Y. Xia, *Angew. Chem.* **2009**, *121*, 2765; *Angew. Chem. Int. Ed.* **2009**, *48*, 2727.
[18] A. Raman, M. Dubey, I. Gouzman, E. S. Gawalt, *Langmuir* **2006**, *22*, 6469.
[19] D. Burdinski, M. Saalmink, P. W. G. van den Berg, C. van der Marel, *Angew. Chem.* **2006**, *118*, 4461; *Angew. Chem. Int. Ed.* **2006**, *45*, 4355.
[20] Y. Xia, G. M. Whitesides, *Angew. Chem.* **1998**, *110*, 568; *Angew. Chem. Int. Ed.* **1998**, *37*, 550.
[21] P. E. Laibinis, G. M. Whitesides, D. L. Allara, Y.-T. Tao, A. N. Parikh, R. G. Nuzzo, *J. Am. Chem. Soc.* **1991**, *113*, 7152.
[22] K. S. Suslick, *Science* **1990**, *247*, 1439.
[23] M. Fell, S. M. Murphy, *J. Nucl. Mater.* **1990**, *172*, 1.
[24] A. K. Khurana, H. Chen, C. G. Wall, *Chem. Eng. Commun.* **1998**, *165*, 199.
[25] C. E. Brennen, *Cavitation and Bubble Dynamics*, Oxford University Press, Oxford, **1995**.
[26] M. Blander, J. L. Katz, *AlChE* **1975**, *21*, 833.
[27] T. J. Mason, *Chem. Soc. Rev.* **1997**, *26*, 444.
[28] *CRC*, *Handbook of Chemistry and Physics*, 85th ed., CRC, Boca Raton, FL, **2004–2005**.
[29] J. P. J. Nail, R. I. Vachon, J. Morehouse, *Trans. ASME. J. Heat Transfer* **1974**, *96*, 132.
[30] J. R. Blake, G. S. Keen, R. P. Tong, M. Wilson, *Philos. Trans. R. Soc. London Ser. A* **1999**, *357*, 251.
[31] E. A. Brujan1, T. Ikeda, Y. Matsumoto, *Phys. Med. Biol.* **2005**, *50*, 4797.
[32] B. M. Borkent, S. Gekle, A. Prosperetti, D. Lohse, *Phys. Fluids* **2009**, *21*, 102003.
[33] L. B. Goetting, T. Deng, G. M. Whitesides, *Langmuir* **1999**, *15*, 1182.
[34] Materials Safety Data Sheet for Aluminum Etchant Type A, Transene Co. Inc. Danvers Industrial Park. 10 Electronics Avenue, Danvers, MA 01923.
[35] Free Software Foundation GNU General Public License. Web site: http://www.gnu.org/licenses/licenses.html#GPL.

